AD-A096 391 MASSACHUSETTS INST OF TECH LEXINGTON LINCOLN LAB F/G 5/8
RADC MULTI-DIMENSIONAL SIGNAL-PROCESSING RESEARCH PROGRAM.(U)
SEP 80 D E DUDGEON F19628-80-C-0002

UNCLASSIFIED ESD-TR-80-218 NL

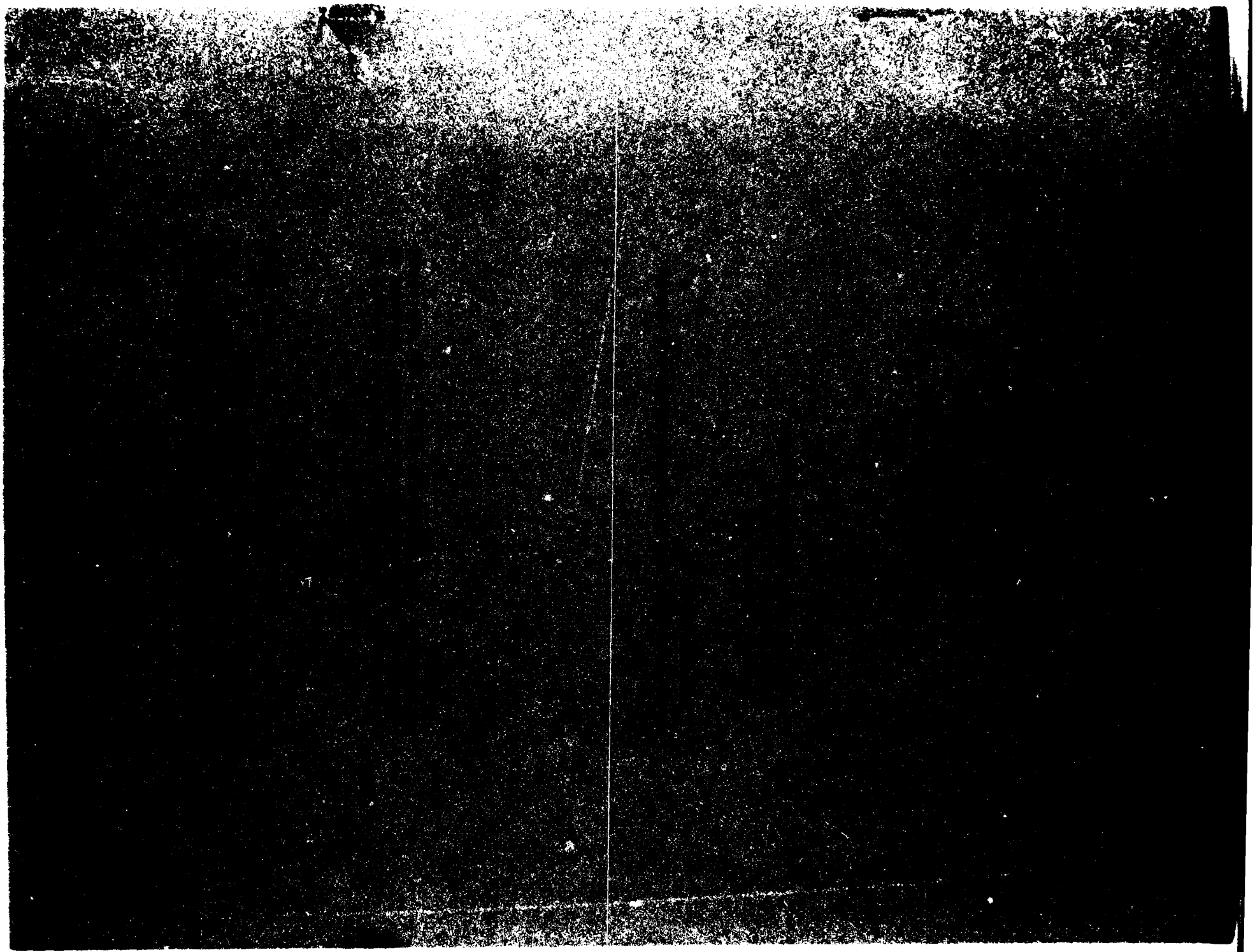

MASSACHUSETTS INSTITUTE OF TECHNOLOGY
LINCOLN LABORATORY

RADC MULTI-DIMENSIONAL SIGNAL-PROCESSING RESEARCH PROGRAM

SEMIANNUAL TECHNICAL SUMMARY REPORT
TO THE
ROME AIR DEVELOPMENT CENTER

1 APRIL – 30 SEPTEMBER 1980

ISSUED 22 JANUARY 1981

LEXINGTON MASSACHUSETTS

ABSTRACT

This Semiannual Technical Summary Report covers the period 1 April through 30 September 1980. It describes the significant results of the Multi-Dimensional Signal-Processing Program in the areas of image modeling, image segmentation and classification, advanced digital filter implementations for image processing, and iterative algorithms for image restoration and enhancement.

The work was carried out with support of the Department of the Air Force; a part of this support was provided by the Rome Air Development Center.

CONTENTS

RADC MULTI-DIMENSIONAL SIGNAL-PROCESSING RESEARCH PROGRAM

1. INTRODUCTION AND SUMMARY

The Lincoln Laboratory Multi-Dimensional Signal-Processing Research Program was initiated in FY 80 as a research effort directed toward the development and understanding of the theory of digital processing of multi-dimensional signals and its application to real-time image processing and analysis. Specific areas of interest include advanced filter and processor architectures for image enhancement, and the modeling of image data for segmentation, classification, and detection. This report discusses technical accomplishments over the last six months in these two areas.

Segmentation and classification are important aspects of the automated analysis of aerial reconnaissance imagery. Our work on segmentation and classification, discussed in Sec. 2 of this report, has focused on the development of statistical models and related algorithms for segmentation/classification. The models, which are based on white-noise-driven linear filters, permit development of the joint probability density function or likelihood function for the image.

With an expression for the likelihood function in hand, segmentation can be regarded as an estimation problem for the image regions. Maximum likelihood estimation leads to a simple segmentation algorithm but one that yields generally unsatisfactory results. The modeling of region transition statistics as a Markov chain allows formulation of the maximum a posteriori (MAP) estimation problem; a solution of the MAP equations can be obtained through an iterative procedure. The MAP approach was found to produce much more satisfactory results. Examples of image segmentation are shown for texture images and for aerial photographs of rural areas.

The discussion in Sec. 3 on the enhancement and filtering of aerial photographs represents a coalescence of work in two different areas, the development of an iterative implementation for 2-D non-causal rational filters and the investigation of techniques for restoring images that have been blurred by a known blurring function. We have found that an iterative restoration algorithm, which is related to the iterative implementation developed previously,[1] works well in removing the effects of blurring.

2. IMAGE MODELING FOR SEGMENTATION AND CLASSIFICATION

2.1 Introduction

The problem of detecting objects in structured backgrounds, such as terrain, is of interest in many applications. Since the image in which the detection is to take place generally consists of many different types of background regions with irregular boundaries, segmentation of the background into regions with homogeneous structure can be an important prerequisite to detection. Further, the classification of background regions is of interest since it may reduce the number of areas that need to be considered for detection of a particular type of object.

During this reporting period, work has focused on the development of statistical models for natural terrain and on the generation of segmentation and classification algorithms based on these models. The models are derived using stochastic filtering concepts and are described in the following subsection; the segmentation and classification algorithms are described in the next two subsections. Examples of segmentation results for texture and terrain images are shown and discussed.

2.2 Modeling of Texture and Terrain Images

Images of interest here are assumed to consist of a number of connected regions each of which contains a texture or terrain of a fixed type. A model for the image can be developed as follows: Within a given region, the image is represented by the output of spatial linear filter driven by white noise (see Fig. 1). If the probability density function for the white noise is known,

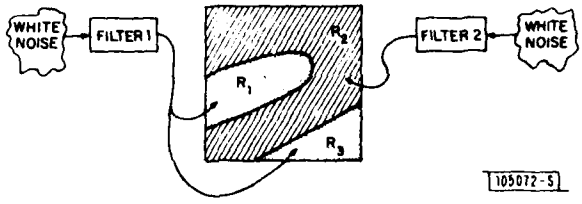

Fig. 1. Model for image consisting of two region types.

then the multivariate probability density function for the set of all points F_i within the region R_i can be computed. Denoting this quantity by $p_k(F_k|R_i)$ where k is the texture type, we can write the multivariate probability density for the image, conditioned on a set of regions $R_1, \ldots, R_N$ as

$$p(F|R_1, \ldots, R_N) = \prod_{i=1}^{N} p_{k_i}(F_i|R_i) \quad . \tag{1}$$

If a causal (quarter-plane) recursive filter and Gaussian white noise are used in the model, then the expression for minus twice the log of the density function is approximately†

$$-2 \ln p_{k_i}(F_i|R_i) \cong \sum_{n,m \in R_i} \left\{ \frac{[E_{k_i}(n,m)]^2}{\sigma_{k_i}^2} + \ln \sigma_{k_i}^2 + \ln 2\pi \right\} \tag{2}$$

where n and m are coordinates of points in the region, $\sigma_{k_i}^2$ is the white noise variance and $E_k(n,m)$ is given by

$$E_k(n,m) \triangleq \sum_{i=0}^{I} \sum_{j=0}^{J} a_{ij}^{(k)} [F(n-i, m-j) - M_k] \quad . \tag{3}$$

Here M_k is the mean of F, $a_{oo}^{(k)} = 1$, and the remaining a_{ij} are the coefficients of the recursive filter. Under these conditions, E_k can be interpreted as the error in linear prediction of the image using the filter of class k. Equation (1) and its explicit realization [Eq. (2)] are the key to the segmentation and classification algorithms described below. Generalizations and further details of the modeling are given in Ref. 2.

2.3 Segmentation as an Estimation Problem

Given an image F, we can regard Eq. (1) as a likelihood function in the parameters N and R_i. A maximization of Eq. (1) with respect to these parameters yields a maximum likelihood (ML)

† The expression neglects boundary effects (see Ref. 2).

estimate for the regions. In view of Eq. (2), maximization of Eq. (1) is equivalent to assigning each point (n, m) in the image to a region R_i (of type k_i) such that the term in brackets is minimized. Specifically, for the case of two region types, we are led to the condition

$$\frac{E_o^2(n,m)}{\sigma^2} + \ln \sigma_o^2 \underset{1}{\overset{0}{\lessgtr}} \frac{E_1^2(n,m)}{\sigma_1^2} + \ln \sigma_1^2 \quad . \tag{4}$$

The double inequality sign indicates that a point (n, m) is assigned to region 0 if the left-hand expression is less than the right-hand one and assigned to region 1 if the opposite is true.

Since the ML estimate assigns points to texture types without regard to the assignments of adjacent points, the procedure tends to produce a poor estimate for the regions. Figure 2(a) shows a composite of two random textures in three connected regions. In this example, there is no difference in the mean gray level for the two types of textures. Figure 2(b) shows the ML segmentation obtained by assigning pixels to black or white levels (texture types 0 and 1, respectively). Although the outline of the true regions is discernible to a human observer the procedure has in fact generated many false regions.

A better procedure is to use some form of Bayes estimation. From our arguments with respect to the ML estimate, we can observe that a segmentation $\{R_1, R_2, \ldots, R_N\}$ of the image is completely equivalent to an assignment of the pixels to 0 and 1. We shall refer to such an assignment for a point (n, m) as its "state" $s_{n,m}$ and let that state be stochastically dependent on the values of states in a surrounding region $S_{n,m}$. In particular, following Kaufman et al.[3] we assume that the states form a Markov chain with transition probabilities $\Pr[s_{n,m}|S_{n,m}]$. By combining Eq. (1) and the transition probabilities, and applying Bayes' rule, we can form the posterior probability of the state assignment. Maximizing this expression leads to a MAP estimate for the regions. By taking logarithms and eliminating constant terms, we find that an equivalent statement of the MAP estimation problem is to minimize the expression

$$\sum_{(n,m)} \frac{E_{s_{n,m}}(n,m)^2}{\sigma^2_{s_{n,m}}} + \ln \sigma^2_{s_{n,m}} - 2 \ln \Pr[s_{n,m}|S_{n,m}] \tag{5}$$

over all choices of the $s_{n,m}$. Specifically, in the two-class case, we must satisfy the conditions

$$\frac{E_o^2(n,m)}{\sigma_o^2} + \ln \sigma_o^2 - 2 \ln \Pr[0|S_{n,m}] \underset{1}{\overset{0}{\lessgtr}} \frac{E_1^2(n,m)}{\sigma_1^2} + \ln \sigma_1^2 - 2 \ln \Pr[1|S_{n,m}] \quad . \tag{6}$$

The state interdependence imposed by the Markov model is clear from Eq. (6), but it also renders a direct solution impossible in practice. However, it is possible to set up an iterative procedure where, beginning with the ML state assignments, one fixes the $S_{n,m}$ and uses Eq. (6) to obtain an updated set of state assignments. The updated states are then used for the $S_{n,m}$ in the next iteration.

For the results reported here, the state was taken to be dependent on values in a 5- × 5-pixel square region centered around the point (n, m), and the transition probabilities were taken to be proportional to the number of 1's or 0's present in that region. Figure 2(c) shows the results of this procedure after 16 iterations. Since there is an inherent ambiguity in the estimation of the region boundaries proportional to the size of the support of the autoregressive filters, the edges are somewhat rough. Smoothing with a small-kernel linear filter produces the result shown in

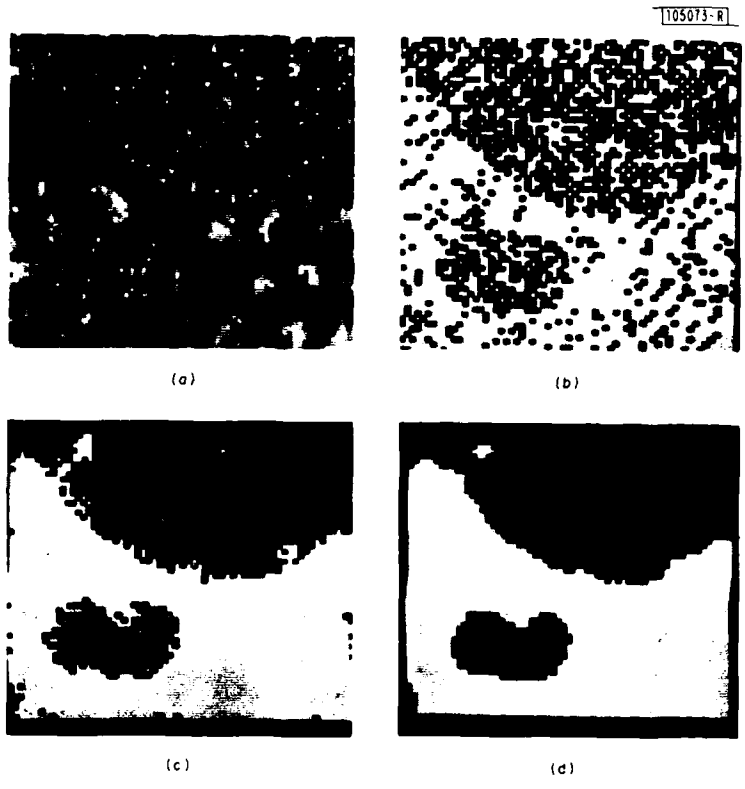

Fig. 2. Segmentation of a texture image: (a) 64 × 64 pixels, (b) ML segmentation, (c) MAP segmentation, and (d) MAP segmentation after smoothing.

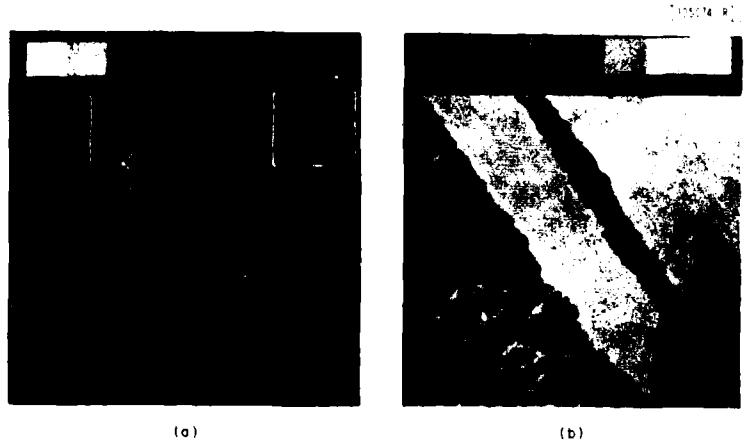

Fig. 3. Aerial photographs of natural terrain (128 × 128 pixels).

Fig. 2(d). The three regions have been identified well except for one small false white area in the upper left corner.

The MAP region estimation procedure was also applied to the aerial photographs of terrain shown in Fig. 3. The goal here is to segment the images into regions of trees and fields without further segmentation with respect to tree or field characteristics. Although both images shown in Fig. 4 represent similar types of data, there are some significant differences between the images particularly with respect to average gray level of the two classes. However, for purposes of these experiments, no normalizing procedures were applied to the data. The filter coefficients for the segmentation and classification were estimated from data in the two white boxes in Fig. 3(a). The MAP algorithm was then applied to the entire images. Figure 4 shows the results of region estimation for the two images. No smoothing of the edges was performed here. Figure 4(a) shows generally solid identification of the two region types. Figure 4(b) shows consistent identification of the fields and most of the trees with some problems occurring in tree areas that are lighter in tone or show longer spatial autocorrelation characteristics.

Fig. 4. MAP segmentation of Fig. 3 images.

As a follow-on experiment, the upper left-hand corner of the image in Fig. 3(a) was further segmented to separate the larger trees from the smaller ones. In the enlarged section shown in Fig. 5(a), it is more difficult to visually identify the image as that of trees but there are noticeable differences in spatial correlations of the textures within the image that are not unlike those seen in the texture image of Fig. 2. The segmented result shown in Fig. 5(b) coincides with most observers' visual segmentation of the tree image and also with the details visible on the original aerial photograph prior to digitization (not shown). This suggests that terrain segmentation might well be performed in a layered, hierarchical manner starting with a segmentation into gross categories and proceeding to increasing levels of detail as required.

2.4 Classification of Presegmented Images

In the preceding section, the goal was to segment an image into known categories and the segmentation and classification proceeded concurrently. In some applications, it may be required

Fig. 5. Segmentation of large and small trees: (a) section of tree and field image and (b) MAP segmentation.

to classify an image consisting of a single type of texture or terrain into one of a set of known categories. Such presegmented but unclassified images may arise as the output of a view of a camera or sensor to an area known to be of homogeneous structure. In this situation, the classification can be addressed in terms of statistical hypothesis testing. Once again, the model and likelihood functions described in Sec. 2.2 play a key role. Classification of the image can be carried out as a fixed sample size test involving the entire set of pixels or as a sequential test using some contiguous subset of pixels. The sequential test may be useful, for example, if the image is being developed in a scan mode and time and resources for classification must be carefully allocated. In either case, the likelihood function is developed in a recursive manner. Additional details of this procedure can be found in Ref. 2.

3. ENHANCEMENT OF AERIAL PHOTOGRAPHY

3.1 Introduction

In this research area, we have devoted our efforts to enhancement and restoration of aerial photographs, and, in particular, the sampled images recently received from RADC/IRRE. Our studies can be categorized in the following way:

(a) Generalizations and applications of the iterative implementation of 2-D digital filters.[1]

(b) A theoretical study of convergence of signal reconstruction algorithms such as phase-only or magnitude-only reconstruction, and band-limited extrapolation.

(c) Estimation of the phase of the Fourier transform of an image for image restoration.

In the first area, we have extended the original formulation of iterative filters so that any stable 2-D rational transfer function can be implemented by an iterative filter. That is, we have extended the class of filters that can be implemented iteratively. This generalization has led to some interesting filter structures for accelerating convergence. In particular, trade-offs between filter complexity and speed of convergence have been empirically demonstrated.

In a more practical vein, we have applied iterative filtering to the problem of image restoration, and in particular, to the problem of image deblurring. In addition, we also have performed

some preliminary studies and experiments on the use of iterative filters in cloud removal, where cloud cover is modeled by both gray-scale modification and blurring due to light scattering.

In the second area of interest, we have formulated a general convergence proof, applicable to a particular class of signal reconstruction algorithms.[4] Although our development centers on two specific examples, band-limited extrapolation and phase-only reconstruction, our approach is general and may be applied to other iterative algorithms that satisfy the same assumptions. Our technique yields the first proof of convergence for the phase-only reconstruction algorithm and may be easily generalized to multi-dimensional signals. Furthermore, the method of proof can be used with nonlinear constraints such as positivity and with modifications for accelerating convergence. Our studies also have led to some interesting observations on the relationship between iterative filters and iterative reconstruction.

The final area of investigation is phase estimation, and phase determination from intensity measurements. This work can be classified as follows:

(a) Determining the phase of a complex wavefront from multiple intensity measurements.

(b) Estimation of the phase of an image in the presence of additive noise.

The first approach is useful when a coherent optical imaging system yields a misfocused image. The second area is applicable in enhancing images degraded, for example, by quantization noise or film graininess.

3.2 Generalizations and Applications of Iterative Filters

The original motivation for an iterative implementation of 2-D digital filters was to build up a complicated impulse response from simple convolutions with impulse responses of finite extent. Such an implementation is well suited to highly parallel array architectures. Another motivation is the implementation of non-causal rational transfer functions. Image restoration, for example, often requires a non-causal inverse filter.

The iterative filtering procedure[1] can be viewed as a 1st-order feedback loop, where a filtered version of the input image is added to a filtered version of the result of the previous iteration. A generalization of this structure can be derived in a way similar to the original derivation.

3.2.1 A Generalized Formulation

A 2-D rational frequency response can be written as

$$H(\omega_1, \omega_2) = A(\omega_1, \omega_2)/B(\omega_1, \omega_2) \tag{7}$$

where $A(\omega_1, \omega_2)$ and $B(\omega_1, \omega_2)$ are trigonometric polynomials. In generalizing the original iteration, we define the function

$$C(\omega_1, \omega_2) = 1 - \lambda(\omega_1, \omega_2)\, B(\omega_1, \omega_2) \tag{8}$$

where $\lambda(\omega_1, \omega_2)$ is a trigonometric polynomial. If we define $X(\omega_1, \omega_2)$ as the spectrum of the filter's input signal $x(n_1, n_2)$ and $Y(\omega_1, \omega_2)$ as the spectrum of the filter's output signal $y(n_1, n_2)$, then from Eqs. (7) and (8) we can derive an implicit relation for $Y(\omega_1, \omega_2)$:

$$Y(\omega_1, \omega_2) = \lambda(\omega_1, \omega_2)\, A(\omega_1, \omega_2)\, X(\omega_1, \omega_2) + C(\omega_1, \omega_2)\, Y(\omega_1, \omega_2) \quad . \tag{9}$$

This implicit formula suggests the iterative formulation:

$$Y_i(\omega_1, \omega_2) = \lambda(\omega_1, \omega_2)\, A(\omega_1, \omega_2)\, X(\omega_1, \omega_2) + C(\omega_1, \omega_2)\, Y_{i-1}(\omega_1, \omega_2) \quad . \tag{10}$$

The iterative solution will converge to the desired filter output providing

$$|C(\omega_1, \omega_2)| < 1 \quad . \tag{11}$$

In fact, unlike with the original iteration [where $\lambda(\omega_1, \omega_2) = 1$], it is straightforward to demonstrate that this condition can always be made to hold with an appropriate choice of $\lambda(\omega_1, \omega_2)$. For example, when

$$\lambda(\omega_1, \omega_2) = \alpha B^*(\omega_1, \omega_2) \tag{12}$$

where α is a scalar such that

$$0 < \alpha < 2 \max |B(\omega_1, \omega_2)|^2 \tag{13}$$

then, $|C(\omega_1, \omega_2)| < 1$ for all (ω_1, ω_2).

3.2.2 *Methods of Accelerating Convergence*

Equation (13) suggests a means of accelerating the convergence of the iteration given by Eq. (11). Since the convergence rate increases as $|C(\omega_1, \omega_2)|$ approaches zero, we wish to choose the parameters of $\lambda(\omega_1, \omega_2)$ so that

$$|C(\omega_1, \omega_2)| = |1 - \lambda(\omega_1, \omega_2)\, B(\omega_1, \omega_2)| \approx 0 \tag{14}$$

or equivalently

$$\lambda(\omega_1, \omega_2) \approx 1/B(\omega_1, \omega_2) \quad . \tag{15}$$

If we consider $\lambda(\omega_1, \omega_2)$ to be the frequency response of a 2-D filter, we can drive $C(\omega_1, \omega_2)$ closer to zero by allowing the spatial extent of that filter's impulse response to grow. Thus, a trade-off exists between filter complexity and convergence rate.

From a slightly different point of view, suppose we want to implement the filter $1/B(\omega_1, \omega_2)$ and suppose $\lambda(\omega_1, \omega_2)$ is a poor approximation to $1/B(\omega_1, \omega_2)$. Then, using the iteration given by Eq. (11), we can improve the result of the filtering operation to achieve a better realization of $1/B(\omega_1, \omega_2)$.

3.2.3 Application to Image Deblurring

Let's now assume that an image $i(n_1, n_2)$ has been blurred by a finite extent Gaussian-shaped blurring function $b(n_1, n_2)$ to give a blurred image $x(n_1, n_2)$. In the frequency domain, we have

$$X(\omega_1, \omega_2) = I(\omega_1, \omega_2)\, B(\omega_1, \omega_2) \quad . \tag{16}$$

The desired image is, of course,

$$Y(\omega_1, \omega_2) = I(\omega_1, \omega_2) = X(\omega_1, \omega_2)/B(\omega_1, \omega_2) \tag{17}$$

and thus the filter $H(\omega_1, \omega_2)$ to be implemented is

$$H(\omega_1, \omega_2) = 1/B(\omega_1, \omega_2) \quad . \tag{18}$$

An original RADC image and its artificially blurred counterpart are shown in Fig. 6.

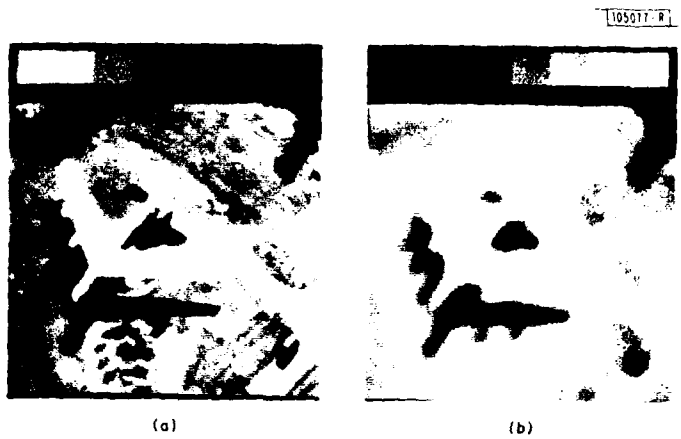

Fig. 6. (a) Original and (b) blurred RADC image.

Since $B(\omega_1, \omega_2)$ takes on very small values in high-frequency regions, $H(\omega_1, \omega_2)$ will take on exceedingly large values in these regions, and consequently will be very sensitive to any noise. The result of applying a direct inverse filter to $X(\omega_1, \omega_2)$ is shown in Fig. 7 along with the blurred image. Note the severe degradation due to high-frequency sensitivity.

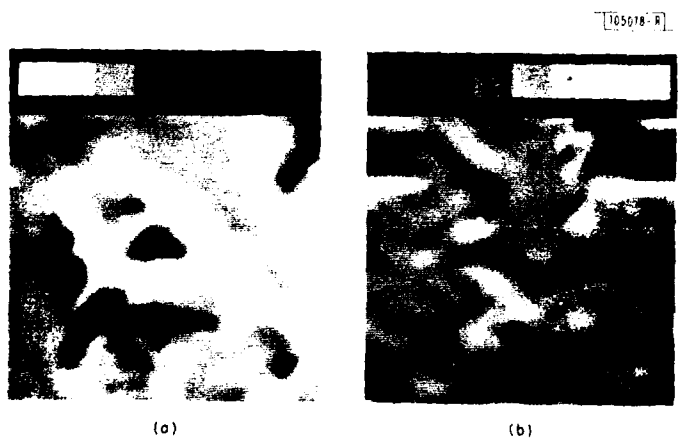

Fig. 7. (a) Blurred RADC image and (b) reconstruction by direct inverse filtering.

The iterative approach, on the other hand, slowly builds up the desired inverse filter and seems to avoid the sensitivity problem inherent in the direct approach. Figure 8(a) shows a blurred image and (b) illustrates the restored image after 20 iterations with $\lambda(\omega_1, \omega_2)$ set equal to a constant. When $\lambda(\omega_1, \omega_2)$ is allowed to vary (a filter of length equal to that of $B(\omega_1, \omega_2)$ was designed), fewer iterations were required to obtain a slightly better restoration. Figure 9(a) depicts the blurred image and (b) the restored image after only 10 iterations when the variable $\lambda(\omega_1, \omega_2)$ was applied. This example demonstrates the trade-off between the spatial extent (or complexity) of $\lambda(\omega_1, \omega_2)$ and the convergence rate.

(a) (b)

Fig. 8. (a) Blurred RADC image and (b) reconstruction by iterative filtering with fixed λ and 20 iterations.

(a) (b)

Fig. 9. (a) Blurred RADC image and (b) reconstruction by iterative filtering with variable λ and 10 iterations.

3.2.4 Extensions

The theoretical and empirical results of the previous subsections have led to a number of interesting possible extensions. First, under certain conditions, the generalized formulation can be shown to yield the phase of the desired (filtered) image after only one iteration. Since, for a certain class of images, all the information lies in the phase, we might conclude that after only one iteration, we have restored the desired information. This phase information, therefore, may be useful in increasing the convergence rate or perhaps in reducing the noise buildup as the iteration proceeds.

Another important insight we have recently made is that the iteration of Eq. (11) can be slightly modified to take on the appearance of the more traditional iterative signal reconstruction algorithms such as the Gerchberg[5] and Van Cittert[6] algorithms. As a result, it is possible to view an iterative filter as an iterative reconstruction algorithm so that procedures used within these more traditional approaches can be applied to our problem. For example, we are considering imposing finite extent and positivity constraints on the output of each iteration.

3.3 Convergence of Iterative Signal Reconstruction Algorithms

Imposing finite extent and positivity constraints, as described in the previous subsection, leads into issues of the convergence of a modified version of the iteration given by Eq. (11). More generally, there exist many iterative procedures for signal reconstruction which impose such constraints in the space domain and also makes use of known information in the frequency domain. For example, often only the low-pass region of the spectrum of an image is given. In this case, we would attempt to retrieve resolution by iteratively incorporating the low-pass information in the frequency domain, and the known extent and positivity in the space domain. Furthermore, if in addition to being low-pass filtered, the data are also degraded by a known zero-phase blurring function, only the phase of the low-pass region may be accurately preserved. An iteration had been developed for recovering the desired image from this phase information.[7,8] More recently, we have developed a proof of convergence for this phase-only iteration.[4] The generality of the proof allows for nonlinear constraints such as positivity and minimum or maximum value constraints, and also encompasses a large class of iterative procedures which are based on a nonexpansive mapping.

3.3.1 Nonexpansive Reconstruction Algorithms

The convergence proof relies on the property that an iterative reconstruction procedure is based on a nonexpansive mapping. Heuristically, a nonexpansive mapping defined on a set of images has the characteristic that when any two images, x and y, are operated on by the mapping, the resulting images are "closer" to one another in a mean-squared sense. Letting $d(x, y)$ denote the mean-squared distance between two images, we say a mapping F is nonexpansive if

$$d(Fx, Fy) \leq d(x, y) \quad . \tag{19}$$

(Fx denotes the mapping F applied to the image x.)

The class of algorithms we have dealt with are strictly nonexpansive; that is,

$$d(Fx, Fy) < d(x, y) \quad \text{when } x \neq y \quad .$$

This strict nonexpansiveness property has been proven for both the phase-only reconstruction iteration and also the band-limited extrapolation iteration.[4] More generally, it is of major

importance in proving convergence of a class of iterative algorithms of the form

$$x_{k+1} = Fx_k \quad . \tag{20}$$

Moreover, it marks a significant difference from the contraction property which has been widely used in the literature for proving the convergence of iterative procedures based on contraction mappings.

3.3.2 Convergence of the Under-Relaxed Iteration

One important consequence of our approach is that convergence can be demonstrated for a modified form o Eq. (20) (Refs. 4 and 9). For example, the phase-only iteration can be modified to accelerate convergence by forming the "under-relaxed" version of the iteration given by

$$x_{k+1} = (1 - \lambda)\, x_k + \lambda F x_k \quad ; \tag{21}$$

with appropriate choice of λ, Eq. (21) converges faster than the iteration [Eq. (20)]. The generalized iteration with variable λ also can be put in the form of Eq. (21). As a result, the convergence of certain accelerated versions of the iterative filter implementation may be proved.

3.4 Phase Estimation for Image Restoration

The final topic to be discussed involves techniques of determining phase information from intensity measurements. We have derived a recursive procedure for generating phase information from intensity measurements in more than one plane. The derivation is given in 1-D, but it is easily extended to 2-D. This solution has potential application to focusing a misfocused image formed by a coherent imaging system.

Suppose a complex signal x(n) is the input of a linear space-invariant filter with impulse response h(n). Then

$$y(n) = \sum_k h(n - k)\, x(k) \tag{22}$$

where y(n) is the filter output. When the magnitude functions $|y(n)|$ and $|x(n)|$ are known, a recursive algorithm can be derived for generating all possible sequences x(n) and thus all possible phase functions associated with $|x(n)|$.

The recursive solution is described in the following way. Letting r and i denote "real and imaginary part of," respectively, we must solve the set of equations for $x_r(n)$ and $x_i(n)$ given by

$$x_r(n)\, d_r(n) - x_i(n)\, d_i(n) = c(n) \tag{23a}$$

$$|x(n)|^2 = x_r^2(n) + x_i^2(n) \tag{23b}$$

where $x(n) = x_r(n) + jx_i(n)$, and where $d_r(n)$, $d_i(n)$, and c(n) are functions of h(n), $|x(n)|$, $|y(n)|$, and the previous values of x(n), i.e., x(m), $m = 0, 1 \ldots n - 1$. It is straightforward to see from Eqs. (23a) and (23b) that there exist two possible solutions for x(n). We choose one of the two possible values of x(n) and proceed to compute x(n + 1). Different selections of x(n) at each step will result in different estimates of x(n), but sequences which are compatible with the known magnitude functions $|x(n)|$ and $|y(n)|$.

One approach to removing this two-solution ambiguity is to assume the presence of a second filter acting upon x(n), and that the magnitude of its output is known. With this second filter, a necessary and sufficient condition on the two filters was derived for generating a unique solution for x(n).

One potential application of the recursive solution is the reconstruction of a complex propagating coherent wavefront from intensity measurements in two or more planes. The 2-D filter in this case represents the propagation phenomenon between planes.

The recursion can be used to generate the complex waveform along one plane. The 2-D filter can then be used to "propagate" coherent light to any other plane in space. For example, if an image along a particular plane is out of focus, the filter simulation can theoretically bring the image into focus at some other plane.

REFERENCES

1. D. E. Dudgeon, "An Iterative Implementation for 2-D Digital Filters," Technical Note 1980-6, Lincoln Laboratory, M.I.T. (6 February 1980), DDC AD-A085589.
2. C. W. Therrien, "Linear Filtering Models for Texture Classification and Segmentation," Proc. 5th International Joint Conference on Pattern Recognition, Miami Beach, Florida, December 1980.
3. H. Kaufman, J. W. Woods, V. K. Ingle, R. Mediavilla, and A. Radpour, "Recursive Image Estimation: A Multiple Model Approach," Proc. 18th Conference on Decision and Control, Fort Lauderdale, Florida, 12-14 December 1979.
4. V. T. Tom, T. F. Quatieri, M. H. Hayes, and J. H. McClellan, "Convergence of Iterative Nonexpansive Signal Reconstruction Algorithms," Technical Note 1980-21, Lincoln Laboratory, M.I.T. (1 August 1980), DTIC AD-A090689.
5. R. W. Gerchberg, "Super-resolution through Error Energy Reduction," Opt. Acta 21, 709-720 (1974).
6. P. H. Van Cittert, "Zum Emfluss der Spaltbneite auf die Intensitatswerteilung in Spektrallinien II," Z. Phys. 69, 298-308 (1931).
7. M. H. Hayes, J. S. Lim, and A. V. Oppenheim, "Signal Reconstruction from Phase or Magnitude," Technical Note 1979-64, Lincoln Laboratory, M.I.T. (18 September 1979), DDC AD-A078745.
8. T. F. Quatieri and A. V. Oppenheim, "Iterative Techniques for Minimum Phase Signal Reconstruction from Phase or Magnitude," Technical Note 1980-34, Lincoln Laboratory, M.I.T. (1 August 1980), DTIC AD-A091111.
9. M. H. Hayes and V. T. Tom, "Adaptive Acceleration of Iterative Signal Reconstruction Algorithms," Technical Note 1980-28, Lincoln Laboratory, M.I.T. (to be published).

UNCLASSIFIED

SECURITY CLASSIFICATION OF THIS PAGE *(When Data Entered)*

REPORT DOCUMENTATION PAGE		READ INSTRUCTIONS BEFORE COMPLETING FORM
1. REPORT NUMBER ESD-TR-80-218	2. GOVT ACCESSION NO. AD-A096391	3. RECIPIENT'S CATALOG NUMBER
4. TITLE *(and Subtitle)* RADC Multi-Dimensional Signal-Processing Research Program		5. TYPE OF REPORT & PERIOD COVERED Semiannual Technical Summary 1 April – 30 September 1980 6. PERFORMING ORG. REPORT NUMBER
7. AUTHOR*(s)* Dan E. Dudgeon		8. CONTRACT OR GRANT NUMBER*(s)* F19628-80-C-0002
9. PERFORMING ORGANIZATION NAME AND ADDRESS Lincoln Laboratory, M.I.T. P.O. Box 73 Lexington, MA 02173		10. PROGRAM ELEMENT, PROJECT, TASK AREA & WORK UNIT NUMBERS Program Element No. 62702F Project No. 4594
11. CONTROLLING OFFICE NAME AND ADDRESS Rome Air Development Center Griffiss AFB, NY 13440		12. REPORT DATE 30 September 1980 13. NUMBER OF PAGES 17
14. MONITORING AGENCY NAME & ADDRESS *(if different from Controlling Office)* Electronic Systems Division Hanscom AFB Bedford, MA 01731		15. SECURITY CLASS. *(of this report)* Unclassified 15a. DECLASSIFICATION DOWNGRADING SCHEDULE

16. DISTRIBUTION STATEMENT *(of this Report)*

Approved for public release; distribution unlimited.

17. DISTRIBUTION STATEMENT *(of the abstract entered in Block 20, if different from Report)*

18. SUPPLEMENTARY NOTES

None

19. KEY WORDS *(Continue on reverse side if necessary and identify by block number)*

image classification
iterative image restoration
image segmentation
iterative filtering

20. ABSTRACT *(Continue on reverse side if necessary and identify by block number)*

This Semiannual Technical Summary Report covers the period 1 April through 30 September 1980. It describes the significant results of the Multi-Dimensional Signal-Processing Program in the areas of image modeling, image segmentation and classification, advanced digital filter implementations for image processing, and iterative algorithms for image restoration and enhancement.

The work was carried out with support of the Department of the Air Force; a part of this support was provided by the Rome Air Development Center.

DD FORM 1 JAN 73 1473 EDITION OF 1 NOV 65 IS OBSOLETE

UNCLASSIFIED

SECURITY CLASSIFICATION OF THIS PAGE *(When Data Entered)*

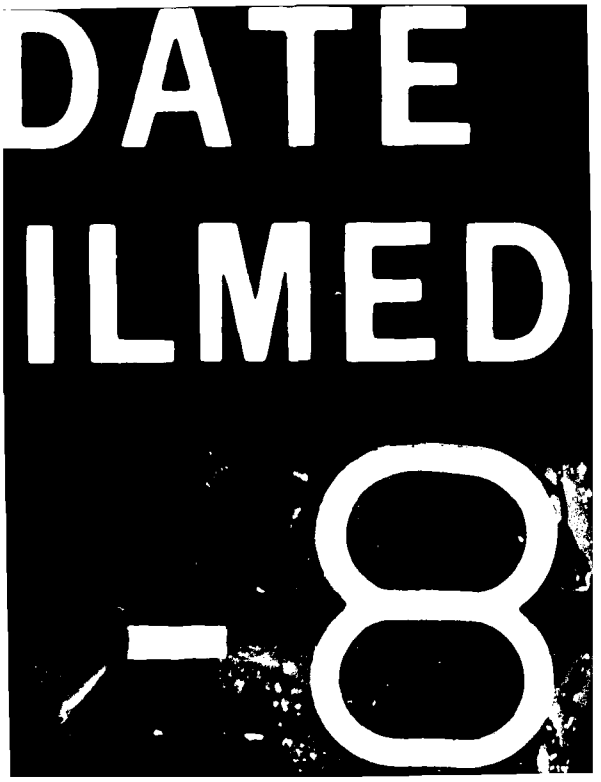
DATE
ILMED
-8